

Harnessing Magnetic-Field Driven Actuation for Microscale Motion in MEMS-Inspired Device

CNF Project Number: 2866-20

Principal Investigator(s): Amal El-Ghazaly

User(s): Ludovico Cestarollo, Zexi Liang, Conrad Smart

Affiliation(s): Electrical and Computer Engineering, Materials Science and Engineering, Lab of Atomic and Solid State Physics; Cornell University

Primary Source(s) of Research Funding: National Science Foundation

Contact: ase63@cornell.edu, lc942@cornell.edu, zl467@cornell.edu, cs2239@cornell.edu

Research Group Website: <https://vesl.ece.cornell.edu>

Primary CNF Tools Used: Heidelberg Mask Writer – DWL2000, SUSS MicroTec Gamma Cluster Tool, ASML PAS 5500/300C DUV Wafer Stepper, Oxford ALD FlexAL, Plasma-Therm Takachi HDP-CVD, Oxford 81/82/100 ICP and PT770 Etchers, Xactix XeF₂ Isotropic Silicon Etch System, DISCO Dicing Saw, Zeiss Ultra SEM, AFM – Veeco Icon, P7 Profilometer

Abstract:

Accurate small-scale control of magnetic actuation necessitates exact tuning of the magnetic fields and gradients that drive movement. In this study, two control magnets create the local magnetic fields needed to induce microscale deflections of a shuttle (in a micromechanical system) equipped with a soft magnetic element. The magnetization orientation and anisotropy of the magnetic element are optimized to maximize deflection in the ON state and its contrast with the OFF state. To demonstrate the effectiveness of the actuation force, a double-folded beam MEMS structure integrated with the control magnets is designed and fabricated.

Summary of Research:

Magnetic actuation stands out in mechanical systems as it allows the generation of large forces in a contactless manner. Various forms of magnetic actuators exist, including magnetic elastomers for millimeter-scale actuation [1-3] and programmable actuators with nanoscale magnets for creating microscale robots [4]. These studies typically use large NdFeB permanent magnets or electromagnetic coils to generate the necessary magnetic fields. However, integrated solutions are needed where both the actuation driver (generating the magnetic field) and actuated mechanism (moving in response to the field) exist within the same micrometer-scale device. Challenges include miniaturizing the switchable magnetic controls and fabricating microscale devices that respond mechanically to magnetic fields. Thin-film magnets produce fields that extend only short distances, requiring precise design of the geometry of

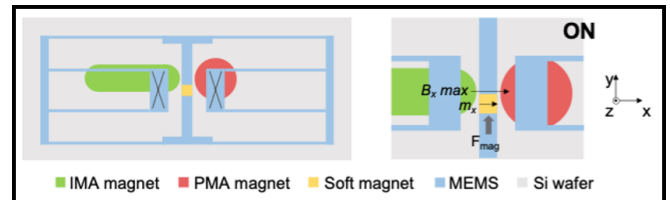


Figure 1: Integrated MEMS featuring a system of beams and magnetic controls.

the actuating mechanism to meet structural constraints. Despite these challenges, magnetic actuation offers a compact, low-power solution for micro-actuators.

This research tackles these issues and presents a tenable design for high-resolution, programmable MEMS micro-actuator. Our novel device uses micro-magnetic controls interacting with a soft magnetic element on a flexible beam system to induce deflection. By programming the magnetization of the control magnets and the soft magnetic element, the system can switch between ON and OFF states. The proposed design features a pair of IMA (in-plane magnetic anisotropy) and PMA (perpendicular magnetic anisotropy) control magnets, as shown in Figure 1.

A double folded beam MEMS is elevated over the magnets, anchored to them by the two supports, each denoted with a cross. The MEMS center shuttle is equipped with a soft magnetic element. This magnet, in response to the field exerted by the two control magnets, imparts a force to the shuttle, causing motion along the y-direction. In the current setup, the presence of a

magnetic field coupling between the control magnets above (or below) their surface corresponds to the ON (and OFF) states.

The control magnets were engineered to obtain the desired anisotropies. The IMA magnet is deposited as a single layer of pure Co in the shape of an elongated ellipse, forcing magnetization along its long dimension purely through shape anisotropy. The PMA magnet, instead, is grown as a Co/Pt heterostructure with 20 repeating layers of nanometer-thick Co and patterned to a circular shape. In the ON state, the IMA and PMA magnets are magnetized in the $+x$ and $-z$ directions, respectively, to concentrate the magnetic flux between them just above their surface. This strong magnetic flux density localization between the two magnets (separated by $1\ \mu\text{m}$) creates a significant B_{xy} ($\partial B/\partial y$) flux density gradient component, inducing a powerful actuation force on the soft magnet (an analytical model was developed to guide the device design). In the complete MEMS actuator, the beams can deflect if the magnetic force overcomes the mechanical restoring force. The mechanical restoring force from the MEMS is calculated by treating it as a system of fixed-guided beams [5]. By fabricating beams with a width (y-direction) of 30 nm and a thickness of 300 nm, and by depositing a soft magnet being 125 nm thick, large deflections up to $1\ \mu\text{m}$ can be achieved.

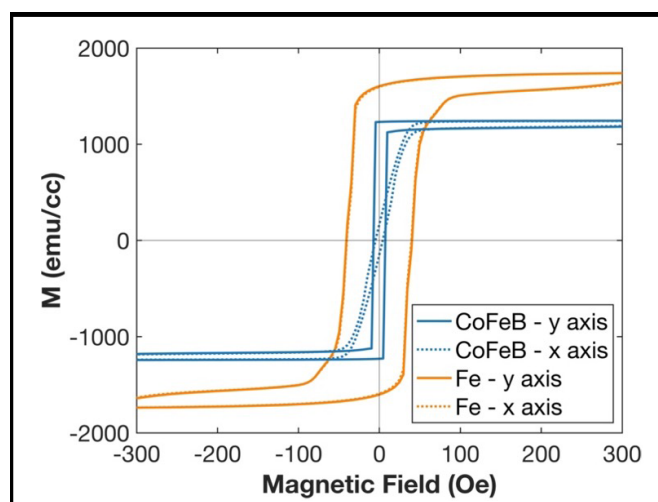


Figure 2: M vs H hysteresis loops along the x and y axes for Fe and CoFeB magnets deposited in the presence of an in-plane magnetic field.

The soft magnetic element was engineered to orient its easy axis along the y -direction in the OFF state, while allowing magnetization in the x -direction when exposed to small fields in the ON state. By depositing a square magnet using $\text{Co}_{43}\text{Fe}_{43}\text{B}_{14}$ in an in-plane field of 200 Oe along the y -direction, the desired behavior with a switching field (H_k) of 40 Oe was achieved, as shown in Figure 2 (this switching can be obtained with the system of IMA/PMA magnets). This switching behavior cannot be replicated with pure Fe, where magnetocrystalline anisotropy is not induced with the application of a field during deposition. As a result, Fe shows identical behavior along the x and y axes due to the absence of shape anisotropy in the square pattern.

Conclusions and Future Steps:

This research paves the way for high-resolution micrometer-scale magnetic actuators. By integrating the magnetic controls (actuating driver) with the MEMS featuring an embedded magnet (actuated mechanism), we are pioneering the development of the first fully-integrated magnetic actuator. Our innovative magnetic design maximizes the contrast in actuation between ON and OFF states. The resulting device, comprising control magnets, a soft magnetic element, and a folded beam MEMS structure, will be the first example of a fully-integrated magnetic actuation system.

References:

- [1] L. Cestarollo, S. Smolenski, and A. El-Ghazaly, "Nanoparticle-based magnetorheological elastomers with enhanced mechanical deflection for haptic displays," *ACS Applied Materials & Interfaces*, vol. 14, no. 16, pp. 19002-19011, 2022.
- [2] Y. Chen, K. Srinivasan, M. Choates, L. Cestarollo, and A. El-Ghazaly, "Enhanced Magnetic Anisotropy for Reprogrammable High-Force-Density Microactuators." *Advanced Functional Materials*, 2305502, 2023.
- [3] S. Marchi, A. Casu, F. Bertora, A. Athanassiou, and D. Fragouli, "Highly magneto-responsive elastomeric films created by a two-step fabrication process," *ACS Applied Materials & Interfaces*, vol. 7, no. 34, pp. 19112-19118, 2015.
- [4] K. Dorsey, T. Pearson, E. Esposito, S. Russell, B. Bircan, Y. Han, M. Miskin, D. Muller, I. Cohen, and Paul L. McEuen, "Atomic layer deposition for membranes, metamaterials, and mechanisms," *Advanced Materials*, vol. 31, no. 29, 1901944, 2019.

Fabrication of Micro Scale Triboelectric Microphone

CNF Project Number: 2929-21

Principal Investigator(s): Shahrzad Towfighian

User(s): Mohammad Alzgoool

Affiliation(s): Mechanical Engineering, Binghamton University

Primary Source(s) of Research Funding: National Science Foundation Grant

Contact: stowfigh@binghamton.edu, malzgoo1@binghamton.edu, mmalzgoool14@gmail.com

Primary CNF Tools Used: Unaxis PT770, OEM AIN Sputtering, AJA Sputter Deposition, Heidelberg DWL-2000 Mask Writer, Oxford PECVD, Oxford 81 Etcher, PT770 Etcher, DISCO Dicing Saw, SÜSS MA6-BA6 Contact Aligner, YES Polyimide Curing Oven, Primaxx Vapor Etcher

Abstract:

In our project, we are trying to fabricate and optimize a microphone that operates by using the mechanical structure and the triboelectric property of polyimide and aluminum with a back-etched wafer with aluminum nitride-aluminum layer as our diaphragm. The back-plate consists of polyimide, aluminum, and amorphous silicon. The motivation of this project comes from the promising results acquired from the MEMS triboelectric accelerometer that gave high signal-to-noise ratio, and the high and linear response of the output voltage [1]. The design from the previous work was optimized for sensitivity by manipulating the dimensions of the serpentine springs of the back-plate, and a back-etch was incorporated into the design to make the device act as a microphone.

Research Summary:

There are many advantages of triboelectric generators over piezoelectric generators such as lower cost, high flexibility, and superior electrical output. The operation of triboelectric generators depends on contact of a metal and a dielectric material with different affinity to electrons, the contact will result in charged conductive plates and separation with high impedance in between the plates will result in high voltage. In this work, we optimized our previous design of triboelectric accelerometers for maximum sensitivity with genetic algorithm [1]. The optimized triboelectric accelerometer was fabricated (Figure 1) and mounted on a shaker. The triboelectric excitation of 2-10 g was applied while the voltage was acquired. Frequency was swept from 0.5- 4 kHz and voltage produced was measured.

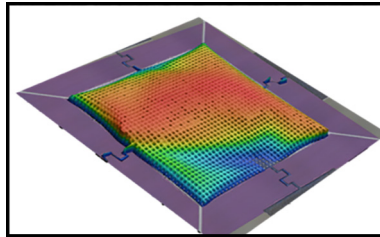


Figure 1: Fabricated triboelectric accelerometer.

Fabrication:

The fabrication process (Figure 2) for triboelectric generator starts with 500 nm aluminum nitride, recipe used for this operation utilized the heater provided with the machine and required seasoning of the wafer for many depositions before continuing with the real wafer. The minimum stress from the nitride layer acquired

with low-stress recipe was -50 MPa while it was more than 1 Gpa for the normal recipe. 500 nm of aluminum is sputtered and patterned for bottom electrode at 3 mtorr with titanium nitride adhesive layer. This is followed by high-rate silicon oxide PECVD layer that is one micron thick to create the gap between upper and lower electrode.

The process is then followed by back etching of the wafer to create inlet for the sound waves, the first aluminum nitride layer acts as a perfect stop-layer for the etching. This is done by cycling 200 loops of etching with five minutes of release to clean black silicon deposits, this process was finalized after 1000 loops. Then, polyimide spin-coating at 5000 rpm for one minute was done, curing by polyimide oven for one hour at 300°C is optimal, and patterning is carried out using RIE oxford 81 with CF_4/O_2 mixture of 15/45 sccm. Then, the top layer is finished by sputtering 200 nm aluminum, which is patterned by PT770 ICP machine, and depositing amorphous silicon for proof-mass with 200°C under 20 mtorr for 20 minutes to ensure stress is within tensile region, the amorphous silicon resulted is one micron thick and is etched with SF_6/O_2 mixture for one minute with RIE machine Oxford 81. Then, release of the top and bottom layers is done by vapor HF etching which is done using slow speed for 2 μm etch followed by 8 μm etch using faster recipe to etch oxide layer sideways. Finally, the wafer is diced and wire-bonded for testing.

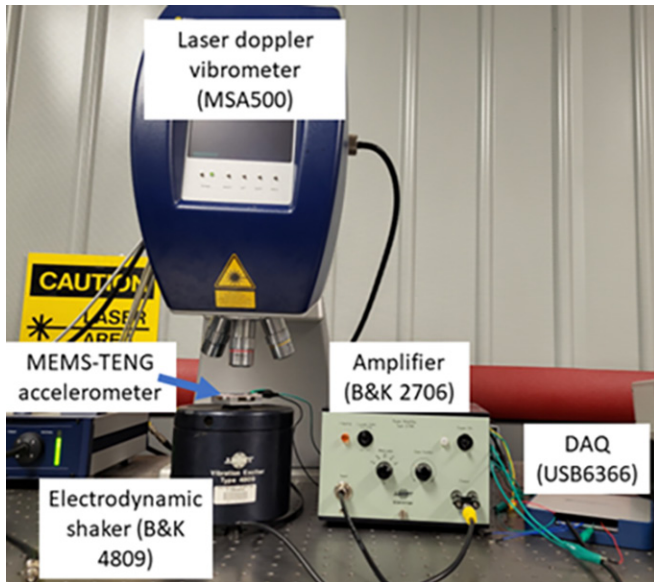


Figure 2: Fabrication process overview.

Results:

The accelerometer was tested at 0.5-4 kHz with excitation amplitude 2-10g with sinusoidal input. The frequency response (Figure 3) shows a noticeable resonance peak at 1.25 kHz with 1.8 V generated at the highest end as a response to excitation of 10g. The frequency response for the rest of the tested bandwidth is relatively flat for every tested acceleration amplitude. The residual stresses during deposition processes of spin-coating the polyimide and from the sputtering deposition of the aluminum layer caused shift in resonance between expected and acquired results. These stresses cause the released membranes to buckle up which creates undesired differences between the designed and the actual device.

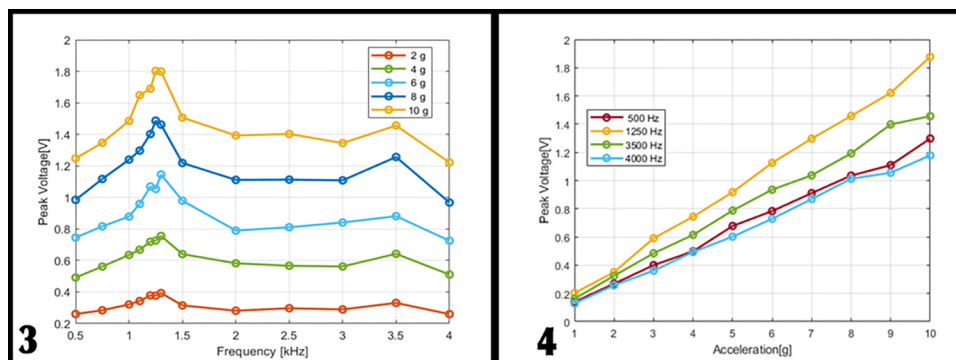


Figure 3: Frequency response of the triboelectric accelerometer.

Figure 4: Excitation amplitude-triboelectric accelerometer output voltage.

Generated voltage-excitation amplitude (Figure 4) still shows linear relation with the highest sensitivity of 187 mV/g. The sensitivity is an improvement over our previous design which has 68 mV/g sensitivity with only 0.7 V as the highest produced voltage [1]. It is also noticed that there is a linear relationship between the measured acceleration and the produced voltage for the fabricated accelerometer at each frequency. Results present a promising design that can be suitable for self-powered MEMS motion sensors or microphones.

Conclusions and Future Work:

In this work, we were able to significantly enhance the performance of a triboelectric accelerometer by applying genetic algorithm to the design and by modifying the fabrication process. We targeted maximum sensitivity in our optimization and changed the placement of the dielectric layer from the bottom to top. The changes made to the fabrication process alongside the changes in the design have improved the device output.

Currently, we are trying to test the device with back-etched volume to act as a microphone. Such work requires complete investigation of both diaphragm and back-plate separately to understand their integration.

References:

- [1] Alzgoor, M., Tian, Y., Davaji, B., and Towfighian, S. (2023). Self-powered triboelectric MEMS accelerometer. *Nano Energy*, 109, 108282.

Magnetically Programmed Diffractive Robotics

CNF Project Number: 2964-21

Principal Investigator(s): Itai Cohen, Paul L. McEuen

User(s): Conrad Smart, Zexi Liang, Melody Xuan Lim, Weiyi Li

Affiliation(s): Kavli Institute at Cornell for Nanoscale Science, School of Applied and Engineering Physics, Laboratory of Atomic and Solid-State Physics, Department of Physics; Cornell University

Primary Source(s) of Research Funding: National Science Foundation, Alfred P. Sloan Foundation

Contact: itai.cohen@cornell.edu, plm23@cornell.edu, cs2239@cornell.edu, zl467@cornell.edu, mxl3@cornell.edu, wl689@cornell.edu

Primary CNF Tools Used: Oxford 81/82 etcher, YES EcoClean Asher, ASML DUV Stepper, Gamma Automatic Coat-Develop Tool, JEOL 9500 EBL, JEOL 6300 EBL, SC 4500 Odd-Hour Evaporator, AJA Sputter Deposition, Heidelberg DWL2000, PT770 Etcher (left side), Unaxis 770 Deep Silicon Etcher, Oxford FlexAL, Oxford PECVD, Plasma-Therm Takachi HDP-CVD, Zeiss SEM, Veeco AFM

Abstract:

We introduce a new class of magnetically controlled microscopic robots (microbots) that operate at the visible-light diffraction limit, which we term diffractive robots. We combine nanometer-thick mechanical membranes, programmable nanomagnets, and diffractive optical elements to create untethered microbots small enough to diffract visible light and flexible enough to undergo complex reconfigurations in millitesla-scale magnetic fields. We demonstrate applications including sub-diffractive imaging using a novel variant of Structured Illumination Microscopy (Robot-SIM, or R-SIM), tunable diffractive optical elements for beam steering and focusing, and force sensing with piconewton sensitivity. This platform offers a powerful new tool for high-resolution imaging, tunable optics, and ultra-small force sensing, merging robotics and optical technologies at the microscale.

wide with varying aspect ratios. The coercive fields and magnetic dipole directions of these nanomagnet arrays are controlled by shape anisotropy [4,5]. The moments align along each magnet's long axis, and higher shape anisotropy (aspect ratio) magnets have higher coercive fields.

Summary of Research:

Microscopic robots with features comparable to the wavelength of light introduce diffractive optical effects, creating exciting new opportunities at the intersection of robotics and optics for probing the microscopic world and controlling light. Although the intersection of diffraction and tunable mechanics have been pioneered in the fields of micro-optical MEMS [1-3], these systems have never been miniaturized into a microscopic robotics package.

The two key elements that enable diffractive robots are programmable nanomagnets and ALD hinges. The nanomagnet arrays consist of single-domain cobalt nanomagnets ~ 100 nm

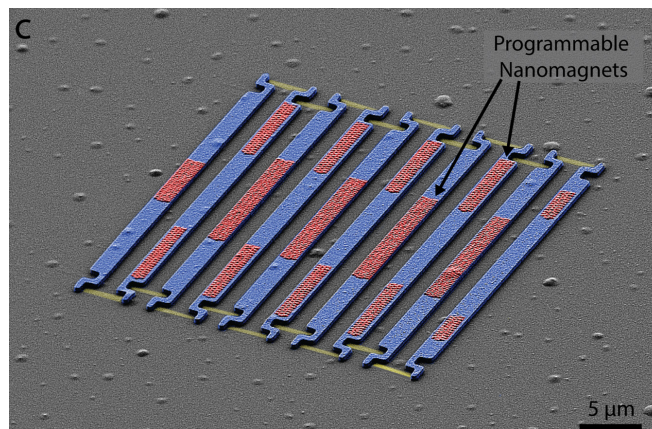


Figure 1: False-color scanning electron microscope image of a diffractive robot, consisting of (yellow) ALD silicon oxide hinges, (red) programmable cobalt nanomagnets, and (blue) rigid silicon oxide panels.

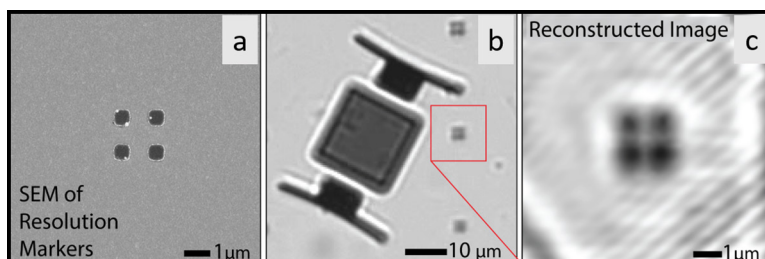


Figure 2: (a) SEM of the 2D resolution markers, (b) micrograph of diffractive robot near markers, (c) R-SIM reconstruction of the markers using the diffractive robot.

Using the disparate coercive fields, we sequentially magnetize the nanomagnet arrays in opposite directions to program the microbot magnetic control. The nanomagnets are embedded in 300 nm thick silicon dioxide panels and capped with chromium. Finally, 5 nm-thick ALD SiO₂ membranes connect the panels (Figure 1) to form a durable flexible joint [6].

As an illustration of the possible applications of diffractive robotics, we use a diffractive robot as a mobile optical element to image beyond the standard diffraction limit of a microscope. We do this using a variant of Structured Illumination Microscopy (SIM), where we use the body of a diffractive robot to create a structured light field, as well as to sample the rotated images for reconstruction. We call this technique Robotic SIM, or R-SIM. Our robot consists of a diffraction grating (1000 lines/mm) body connected to two magnetized panels. We implement R-SIM by walking the robot across the features to be imaged and collecting a series of images at a variety of angles and phases. We demonstrate the power of R-SIM by imaging a pattern of four metal dots spaced 600 nm apart (shown in the SEM in Figure 2a) that cannot be resolved using standard optical microscopy.

The robot is scanned across the feature to collect three angles and five phases per angle, with an overall acquisition time of ~ 30 seconds. The diffraction-limited object in Figure 2b is reconstructed in Figure 2c, demonstrating that R-SIM can resolve the four isolated dots.

To demonstrate beam steering, we fabricate microscopic diffraction gratings with magnetically tunable periodicities as shown in Figure 3. At zero magnetic field, the grating has a periodicity of 500 lines/mm. As the field increases (i-iii) the panels compress. In the corresponding diffraction images, three bright spots are seen: a central bright peak and lesser bright peaks to the left and right which move away from the central peak with increasing magnetic field (i-iii). These peaks are the zeroth, -1, +1 diffractive orders of the grating, corresponding to beams deflected by angles $\theta = \arcsin(n\lambda / a)$, where a is the grating spacing. The mechanical structure of the robot thus allows us to magnetically beam steer the diffractive orders. These gratings can also locomote across the surface to enable mobile, local control of light fields.

Inversely, this coupling between the internal configuration and the optical properties can be used

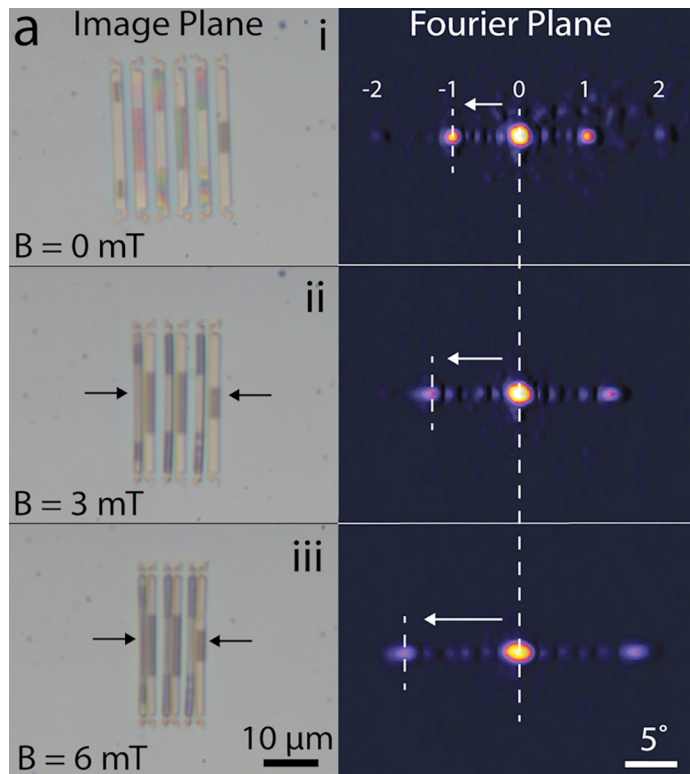


Figure 3: Image plane (left) and Fourier plane (right) of the diffraction grating in a uniform magnetic field of 0 mT, 3 mT, and 6 mT.

to measure small forces acting on the microbot, by measuring the location of the +1 diffractive order. We measure a noise floor of 5 μ T at a 30 Hz bandwidth, with a force sensitivity of 1 pN.

References:

- [1] Z. Yang, T. Albrow-Owen, W. Cai, T. Hasan, Miniaturization of optical spectrometers. *Science* 371, eabe0722 (2021).
- [2] J. Chai, K. Zhang, Y. Xue, W. Liu, T. Chen, Y. Lu, G. Zhao, Review of MEMS Based Fourier Transform Spectrometers. *Micromachines* 11, 214 (2020).
- [3] O. Solgaard, A. A. Godil, R. T. Howe, L. P. Lee, Y.-A. Peter, H. Zappe, Optical MEMS: From Micromirrors to Complex Systems. *Journal of Microelectromechanical Systems* 23, 517-538 (2014).
- [4] J. Cui, T.-Y. Huang, Z. Luo, P. Testa, H. Gu, X.-Z. Chen, B. J. Nelson, L. J. Heyderman, Nanomagnetic encoding of shape-morphing micromachines. *Nature* 575, 164-168 (2019).
- [5] R. P. Cowburn, Property variation with shape in magnetic nanoelements. *J. Phys. D: Appl. Phys.* 33, R1 (2000).
- [6] K. J. Dorsey, T. G. Pearson, E. Esposito, S. Russell, B. Bircan, Y. Han, M. Z. Miskin, D. A. Muller, I. Cohen, P. L. McEuen, Atomic Layer Deposition for Membranes, Metamaterials, and Mechanisms. *Advanced Materials* 31, 1901944 (2019).

Microwave Frequency Acoustic Resonators for Quantum Applications

CNF Project Number: 3042-22

Principal Investigator(s): Andrew Cleland

Affiliation(s): Pritzker School of Molecular Engineering, University of Chicago

Primary Source(s) of Research Funding: AFOSR

Contact: anc@uchicago.edu

Primary CNF Tools Used: OEM Endeavour

Abstract:

We are exploring the low temperature mechanical performance of thin-film, oriented AlN deposited on silicon and sapphire substrates. We are using this material to make bulk acoustic wave and surface acoustic wave devices for quantum applications. These are ultimately for applications in quantum acoustics, to be measured using superconducting qubits as single phonon sources and detectors. The goal is to quantify loss in these devices at low temperatures and low phonon excitation powers.

Summary of Research:

The oriented AlN films we are using are remotely grown by reactive sputter deposition at Cornell's CNF, targeting typically 300 nm thick oriented AlN films. These are then post-deposition patterned with thin-film aluminum at UChicago's PNF, where the patterned aluminum film defines either surface acoustic wave transducers or bulk wave acoustic resonators, with design frequencies in the microwave frequency band (1-10 GHz). At these frequencies, measured at mK temperatures on a dilution refrigerator, these systems will be in their mechanical ground states, so loss and performance can be measured at single phonon powers. The device patterns involve either using geometries with in-plane surface acoustic wave transducers as delay lines or SAW resonators, or using single-sided capacitively-coupled transducers to couple to thickness-mode bulk acoustic wave resonator modes. Devices are measured at low temperatures (10-100 mK) using either microwave frequency vector network analyzers or using superconducting qubits for quantum (single phonon) measurements.

We have demonstrated we can use the AlN films on double-side polished silicon wafers to make high quality factor (1-10 million Q) bulk acoustic wave resonators (BAWs) as measured using a vector network analyzer. We have also integrated similar design BAWs with superconducting qubits to perform measurements in the quantum limit; these experiments are still on-going, with no conclusive results to date.

Conclusions and Future Steps:

Work is still in progress. We may order additional films grown if and when we run out of the existing material.

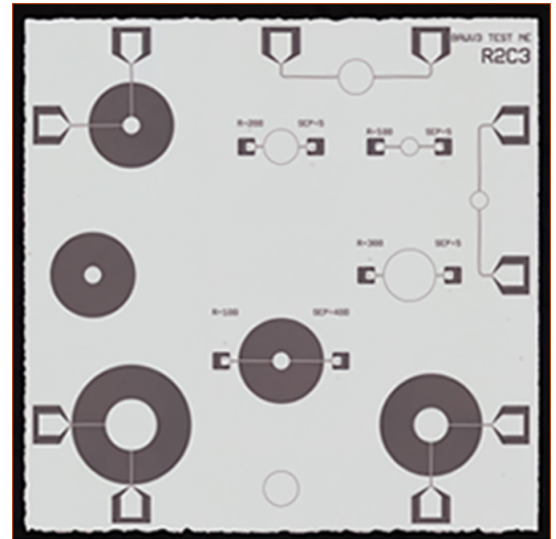


Figure 1: Image of set of bulk acoustic wave resonator structures; silver is aluminum metallization, darker areas are underlying AlN on silicon.

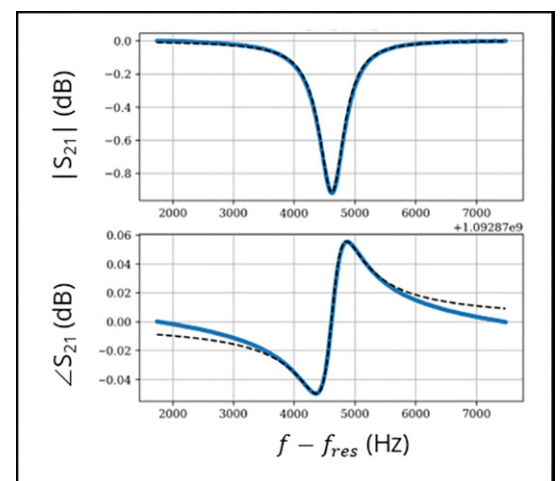


Figure 2: Vector network analyzer measurements of one bulk acoustic wave resonance, with a mechanical Q of about 2 million measured at about 3 GHz and a temperature of 3K.

